

Dosimetric Comparison of IMRT with 3D-CRT Regarding Their Contribution to the Treatment Plan Optimization Using Rando Phantom with a Realistic Lung Cancer Radiotherapy Treatment Planning

Karim Benkahila^{1,2,3}, Fayçal Kharfi^{1,2*}, Fouad Boulakhssaim³, Saad Khoudri³

1. Department of Physics, Ferhat Abbas-Setif1 University, Campus El-Bèz, Setif, Algeria
2. Laboratory of Dosing, Analysis and Characterization in high resolution, Campus El-Bèz, Setif, Algeria
3. Department of Radiotherapy, Fighting against Cancer Medical Centre, Sétif, Algeria

ARTICLE INFO	ABSTRACT
<p>Article type: Original Paper</p> <hr/> <p>Article history: Received: Dec 20, 2019 Accepted: Feb 27, 2020</p> <hr/> <p>Keywords: Radiotherapy Planning Intensity-Modulated Radiotherapy Rando Anthropomorphic Phantom Thermoluminescence Dosimetry Radiotherapy Dosage 3D Conformal Radiotherapy</p>	<p>Introduction: This study compared a three-dimensional conformal radiation therapy (3D-CRT) with a recently implemented intensity modulation radiation therapy (IMRT) technique performed in the irradiation of lung cancer. The objective of this study is to demonstrate the dosimetric advantages of IMRT in target coverage, dose homogeneity, and reducing toxicity.</p> <p>Material and Methods: Depth point doses were compared as calculated by the Varian Eclipse treatment planning system (TPS) on virtual created patient and experimentally measured by thermoluminescence (TL) dosimetry. For treatment planning the same lesion of the real case with different volumes and structures contouring details were created on Rando anthropomorphic phantom computed tomography (CT) data. Dose measurement was performed by calibrated thermoluminescent detectors.</p> <p>Results: The difference between experimental TL measured doses and calculated doses in both techniques show mean values of ~3% (IMRT) and ~1% (3D-CRT) for high dose (>0.55Gy) and ~7% IMRT and 6.5% (3D-CRT) for low dose (<0.55Gy). All IMRT optimized plans improved the heart (-28.3%), the spinal cord (-25.3%), and the left lung (-41.55%) sparing significantly, compared to the 3D-CRT plans. The optimized dose-volume histograms, the dose covering indices, and the dose profile across heterogeneity interfaces showed a significant improvement in dose conformity by IMRT.</p> <p>Conclusion: These findings demonstrate well that TL dosimetry when combined with suitable point dose measurement procedures can efficiently be used as an external and independent dose audit for the comparison between 3D-CRT and IMRT. IMRT with its dose-volume optimization algorithm can achieve a treatment plan quality in lung cancer radiotherapy unachievable by 3D-CRT.</p>

► Please cite this article as:

Benkahila K, Kharfi F, Boulakhssaim F, Khoudri S. Dosimetric Comparison of IMRT with 3D-CRT Regarding Their Contribution to the Treatment Plan Optimization Using Rando Phantom with a Realistic Lung Cancer Radiotherapy Treatment Planning. Iran J Med Phys 2021; 18: 154-163. 10.22038/ijmp.2020.45199.1696.

Introduction

After many recommendations and advice, the intensity-modulated radiotherapy (IMRT) was recently implemented at the Fighting against Cancer Medical Centre (Centre de Lutte Contre le Cancer, [CLCC]), Setif, Algeria. This study was conducted to evaluate IMRT and its contribution to the better treatment of some specific cases of cancers, such as lung cancer, which is unachievable by three-dimensional conformal radiotherapy (3D-CRT). In our previously conducted similar study on 3D-CRT, relatively high dose deviations were observed between calculated and measured doses, particularly in close regions to the heterogeneity interfaces [1]. Although many studies support the use of IMRT in lung cancer, the question is whether IMRT can address such point-dose problems more efficiently

than 3D-CRT, particularly near heterogeneities. However, the implementation of this technique comes with clinical and technical challenges. The IMRT is a more complex technique than 3D-CRT and will certainly need more treatment planning programs in terms of dose calculation and optimization. Therefore, the main reasons for implementing IMRT include the possibility of large treatment volume and the failure to meet organs at risk (OARs) dose constraints by 3D-CRT for such specific cancer cases. In this study, the Eclipse Analytical Anisotropic Algorithm (AAA) 3D-CRT planning tools are combined with interactive dose-to-volume optimization for accurate and effective IMRT planning.

Through this study, it is intended to check if IMRT contributes to fix the problem of heterogeneity

correction and how it contributes to optimal dose covering of the planning treatment volume (PTV) and the OARs sparing. The present study aimed to check the point doses at different depths using the LiF thermoluminescent dosimeter (TLD700) and the Rando phantom following the same procedure for 3D-CRT described by Bouacid et al. [1]. Moreover, it was attempted to examine the compatibility of the dose-volume optimization algorithm used in IMRT planning to reduce the heterogeneity effect in some special regions, such as heterogeneities interfaces. It is also aimed to check if the treatment plans validated during the calculation phase were valid by TL dosimetry according to the International Commission on Radiation Units and Measurements (ICRU) recommendations on dose delivery to the PTV reported in reports 50 and 62 [2,3].

Materials and Methods

Following the same procedure in our previous study [1], TL dosimetry and in-depth dose verification on anthropomorphic Rando phantom (Radiology Support Devices, Inc) have been carried out again considering the IMRT technique instead of 3D-CRT and the same real patient case of lung cancer. Therefore, the same virtual patient was created within the treatment planning system (TPS) for IMRT treatment with the same structures and lung lesions of the real patient. Based on the prescribed dose of 40 Gy in 20 fractions for the real patient, an IMRT treatment plan and a dose calculation were performed for the virtual patient (Rando phantom) using the AAA with IMRT dose-volume optimization algorithm (Varian Eclipse, 11.0.31) [4].

Calculated doses were also checked through the dose measurement in 19 well-selected positions. The 19 measurement positions, where the thermoluminescent detectors (TLDs) have to be placed, were carefully selected to cover the regions of interest in this study, namely PTV, OARs, and the heterogeneities.

Accordingly, the phantom layers corresponding to the CT-slices Z of 6.3 cm, 9 cm, and 12.3 cm were used in this study (Figure 1).

Virtual patient creation and treatment by IMRT

The same procedure used for IMRT was employed in this study for virtual patient creation and treatment by 3D-CRT [1]. A lung lesion of 1394.1cm³ was delineated on Rando phantom CT-slices which is similar to the real patient CT-data in terms of acquisition parameters. The real patient had been treated with a 3D conformal radiotherapy technique at the radiotherapy center of CLCC-Setif, Algeria, with ballistic details and constraint on the dose mentioned in Table 1. Accordingly, for the actual considered IMRT, new beams and constraints were considered on the PTV (Table 2). The considered IMRT dose-volume optimization objectives are presented in Table 3.

Thermoluminescence dosimetry and TL signal reading

The human tissue equivalent TLD-700 thermoluminescent dosimeters (ThermoFisher, SNO78835) were used in this study for the measurement of the delivered dose. The TLD chips were 3.2×3.2×0.89 mm³. These dimensions were well suitable for dedicated phantom slots. Before using these TLDs for dose measurement, an accurate TL-Dose response curve was established. The Risø TL/OSL-DA-20 luminescence reader (DTU Nutech, Denmark) was used for TL signal reading [5,6]. The experimental TL reading conditions are shown in Table 4. The TL intensity is corrected using Eq.(1) [1].

$$TL_{corr} = TL_{meas} \cdot R \cdot E_i \cdot W_i \cdot P_i \tag{1}$$

where E_i is the element correction factor, R signifies the actual to reference TL measurement ratio for a 2 Gy dose, W_i indicates the TLD weight correction factor, and P_i presents the reading position and calibration correction factor [1].

Table 1. Details of the considered radiotherapy 3D-CRT treatment planning of lung lesion

Beam ID	Technique	Field	Field Size (cm)	Field Weight	Field Rotation	Field Angle	Field Depth (cm)	Field Area (cm ²)	Field Volume (cm ³)	Field MU	Field MU per Gy
Post*	Static	6X	1.084	195	0	0	14.8	15.4	87.8	97	
Post.0	Static	6X	0.066	195	0	0	14.8	15.4	87.8	7	
Post.1	Static	6X	0.076	195	0	0	14.8	15.4	87.8	7	
OAD*	Static	6X	0.231	300	0	0	21.4	14.8	85	23	
OAD.0	Static	6X	0.066	300	0	0	21.4	14.8	85	7	
OAD.1	Static	6X	0.072	300	0	0	21.4	14.8	85	7	
ANT*	Static	6X	0.976	15	0	0	14.3	14.1	88.4	84	
ANT.0	Static	6X	0.079	15	0	0	14.3	14.1	88.4	7	

*Post: posterior, OAD: Oblique Anterior Right, ANT: Anterior, SSD: source to surface distance, MU: Monitor Unit. PTV: planning target volume.

Table 2. Details of the considered radiotherapy IMRT improved treatment planning of lung lesion

Prescribed dose	40 Gy given within 20 fractions (2Gy/fraction)									
Constraint on dose	95% of the dose covers 95% of the PTV									
Number of Fields	3fields									
Beam ID	MLC	Energy (MeV)	Field weight	Gantry rotation (°)	Coll rotation (°)	Couch rotation (°)	Beam X (cm)	Beam Y (cm)	SSD (cm)	MU
POST	Dynamic	6X	1	195	0	0	16.1	15	87.8	364
OAD	Dynamic	6X	1	300	0	0	20.9	14.5	85	209
ANT	Dynamic	6X	1	5	0	0	14.4	14	88.7	275

*Post: posterior, OAD: Oblique Anterior Right, ANT: Anterior, SSD: source to surface distance, MU: Monitor Unit. PTV: planning target volume.

Table 3. Dose-volume optimization objectives

Organ and Structure	Volume (%)	Dose (Gy)	Priority (P)	Resolution (mm)
Heart	0	10 (max.)	200	
	0	42 (max.)		
PTV40	9	39 (min.)	200	
	100	39.8 (min)		
Spinal cord	0	5 (max.)	400	3.0
	30	5 (max.)	300	
Left lung	30	10 (max.)	200	
	20	20 (max.)	200	
Lungs without PTV	30	20 (max.)	200	
	20	30 (max.)	200	
PTV42	0	42 (max.)	200	1.72
Outside PTV	0	40 (max.)	300	4.5

Table 4. Conditions of the thermoluminescence signal reading

Luminescence reading mode	Thermoluminescence
Maximum reading temperature	300 °C
Heating rate	5 °C/s
TL signal sampling	250 points over the range 0 °C to 450°C
TLD annealing conditions	10 minutes at 400°C followed by 15 minutes at 100°C

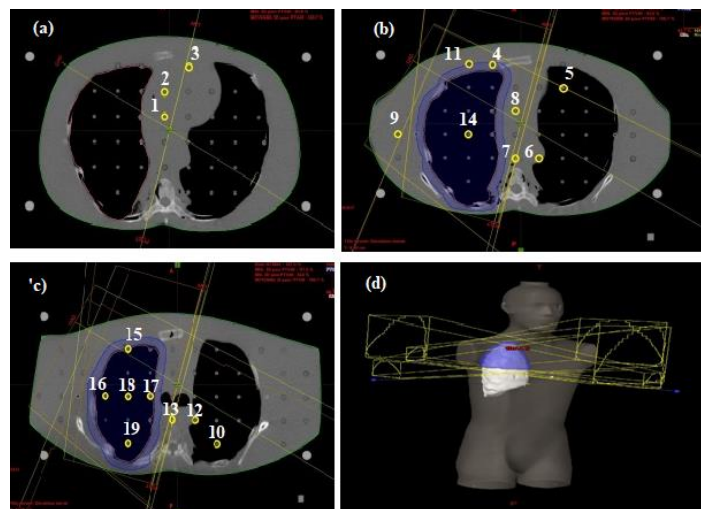


Figure1. Thermoluminescent detector positions shown on CT-slices with radiotherapy beam angles for 3D-CRT: (a) slice with y=6.3cm, (b) slice with y=9cm, (c) slice with y=12.3 cm, (d) 3D fields viewing with PTV (in blue)

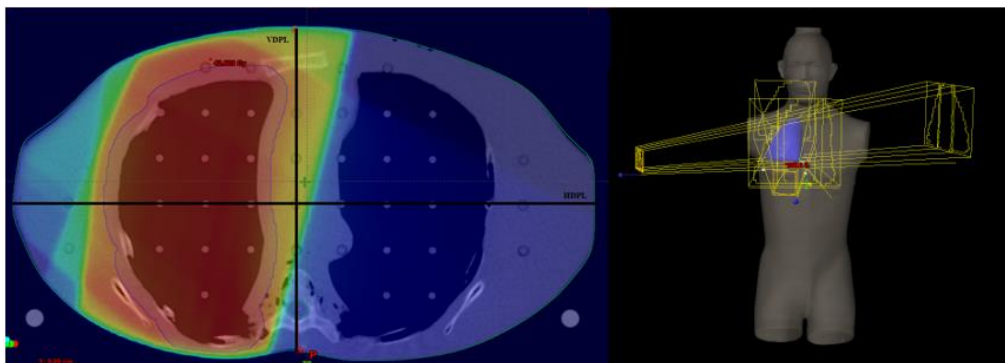


Figure 2. Horizontal dose profile line and vertical dose profile line as selected on CT slice with $y=9\text{cm}$ (solid black lines on the left), 3D Rando phantom with beams used in IMRT (right)

The TLDs were calibrated at the same measurement conditions. The annealing procedure was performed in a suitable oven at two different temperatures (i.e., 400 and 300°C for 15 and 10 min, respectively). The TLDs were placed in the specific inserts of the RW3 water-equivalent slab phantom by avoiding the air gap. The TLDs were irradiated according to the procedure described above to determine the main TL correction factor, and therefore, the TL response curve as a function of dose. The irradiation was performed for a dose of 2 Gy under the reference radiotherapy conditions with a beam field size of $10\times 10\text{ cm}^2$, a depth of 10 cm, and under iso-centric Source-Axis-Distance-set-up ($\text{SAD}=100\text{ cm}$). The TL signal was read just after irradiation. The TL measurement was repeated three times for each TLD. The TLDs with TL intensity standard deviation greater than 3% were excluded from the batch and not used. The mean uncertainty on the TL intensity measurement of all TLDs was obtained at 1.8%. After correcting the TL factor determination, the TL dose-response curve ($\text{TL}=\text{f}[\text{D}]$) was established for the reference TLD for dose varying from 0.1 to 2.5 Gy. To take into account the effect of the irradiation history on the TLDs response, the reference TLD is first irradiated with a dose of 2 Gy dose in any new dosimetry work with the same TLDs batch.

The batch of the TLDs used in this study is composed of 19 TLDs in accordance to the 19 dose-measurement positions (Figures 1 and 2). The dose measurement points were well selected on Rando phantom to cover the PTV, the OARs (heart and spinal cord), and the two sides of heterogonous interfaces (soft tissue/lung). The prescribed dose with the IMRT ballistic and treatment plans summarized in Table 2 was delivered to Rando. Doses were then measured on 19 considered positions. The same protocol used for the TLDs calibration, which includes irradiation, reading, and annealing conditions, was used for dose measurement on Rando phantom.

Dose covering evaluation

To compare dose covering between 3D-CRT and IMRT, the programmed target volume coverage was evaluated using the heterogeneity index, the uniformity index, and the conformity index defined as follows [7]:

$$HI = \frac{D_{2\%} - D_{98\%}}{D_{50\%}} \tag{2}$$

where $D_{2\%}$ is the dose of 2% of the programmed target volume, $D_{98\%}$ presents the dose of 98% of the programmed target volume, and $D_{50\%}$ signifies the dose of 50% of the target volume [7].

$$UI = \frac{D_{5\%}}{D_{95\%}} \tag{3}$$

where $D_{5\%}$ indicates the dose of 5% of the programmed target volume, and $D_{95\%}$ is the dose of 95% of the programmed target volume [8,9].

$$CI = \frac{PTV_{95\%}}{PTV} \tag{4}$$

where PTV is the programmed target volume, and $PTV_{95\%}$ presents the volume covered by 95% of the prescribed dose.

IMRT dose-volume optimization

The AAA is a 3D pencil beam convolution-superposition algorithm. The Varian's TPS *Eclipse* (11.0.31) was used for dose calculation with AAA. In IMRT, the plan quality can be evaluated using either physical or biological criteria. With physical criteria, the IMRT optimization generates conformational dose distributions by modulating field intensities iteratively until the objectives on the dose-volume prescribed in the treatment plan are fully satisfied. The objective function is the sum of the dose-volume objectives defined by the user. The mathematical formulation of the optimization problem is based on the combination of individual quality indicators on target structures and OARs for clinical constraints to yield a single measure that represents the quality of the complete treatment plan. This task is complicated because the given indicators for target structures and organs at risk are linked to interdependent and contradictory optimization goals in terms of maximization and minimization of the delivered dose.

Therefore, the objective function for the target and OAR is simply presented following a weighted sum of individual quality indicators [10,11].

$$F_{T,k} = \frac{1}{N_k} \left[\sum_{i=k}^{N_k} (D_i - D_{p_k})^2 + w_{min_k} \sum_{i=k}^{N_k} (D_i - D_{min_k})^2 \mathcal{H}(D_{min_k} - D_i) + w_{max_k} \sum_{i=k}^{N_k} (D_i - D_{max_k})^2 \mathcal{H}(D_i - D_{max_k}) \right] \tag{5}$$

$$F_{OAR_k} = \frac{1}{N_k} \left[w_{max_k} \sum_{i=k}^{N_k} (D_i - D_{max_k})^2 \mathcal{H}(D_i - D_{max_k}) + w_{dv_k} \sum_{i=k}^{N_{dv_k}} (D_i - D_{dv_k})^2 \mathcal{H}(D_i - D_{dv_k}) \right] \quad (6)$$

In these two last objective functions, the user must define the number of points N_k in the considered PTV or OAR target volume. Optimization is performed for each i^{th} point-dose (D_i) by considering the constraint on dose (Dp_k) for each targeted volume with its minimum and maximum authorized thresholds ($Dmin_k$ and $Dmax_k$). Lower and higher thresholds on dose constraints are weighted with factors $Dmin_k$ and $Dmax_k$. Heaviside function $\mathcal{H}(x)$ is used to ensure that point-dose is considered only if it is in the interval between minimum and maximum dose for the PTV and under the maximum dose and constraint on dose for an OAR. D_{dv_k} is the DVH constraint on the dose of an OAR weighted by w_{dv_k} parameter [10, 11].

Accordingly, the iterative process updated intensity (Ψ^*) and optimized dose (D^*) are given by:

$$\Psi^* = \arg \min_I \left[\sum_j^{N_T} F_{T_j}(D(I), P) + \sum_j^{N_{OAR}} F_{OAR_k}(D(I), P) \right] \quad (7)$$

$$D_i^* = \sum_{j=1}^N K_{ij} J_j^* \quad (8)$$

where P is the set of dose limits and weights for all the optimization structures that define the objective function and K_{ij} presents the dose coefficient (Kernel) corresponding to the j^{th} beamlet and the i^{th} voxel.

Within the Eclipse dose-volume optimization (DVO), the *Gradient* algorithm is used to optimize dose-volume for a given set of parameters P which was initially selected. The selection of P parameters must satisfy the clinical criteria. Automatic methods of P parameter selection have been proposed [12,13]. Stochastic algorithms are also usually used for parameter optimization [14-18]. Eclipse DVO uses automatic P parameter selection with a *Simulated Recruit* method with efficient speed. The iterative optimization stops when the objective function curve varies no longer, the maximum time limit has been reached, the maximum number of iterations has been reached, or dose uniformity in target volumes [19].

The DVO IMRT algorithm was used in this study. This algorithm uses the iterative method to determine the optimal shape and intensity of the field, and therefore, an optimal solution that must conform the dose distribution to the defined user's objectives [20]. The Eclipse DVO (version 11.0.31) is used in the framework of this study. The DVO optimizes the field shape and intensity using simple a deterministic iterative global gradient optimization allowing to find the optimal solution [21]. The dose constraints and the resolution of tissues of interest and OARs were predefined based on the clinical experience and by the direct correlation between clinical observation and characteristic dose values (Table 3). The minimization gradient algorithm is used to optimize dose with global and no local minimums because of the convex shape of the objective function [17]. In this algorithm, a gradient evaluation generates first the gradient direction and length and then the objectives by a line search along the line segment in

order to find the minimum. The main steps of the DVO algorithm are as follows:

1. Field by field optimization
2. Calculation of an intermediate dose for the optimization of plan
3. Calculation of the difference between the intermediate dose and the first optimization result
4. Utilization of the observed difference to compensate for the optimal result in the next iterations
5. Calculation of new intermediate dose and its utilization to compensate next iteration if such case arises
6. Discontinuation of the iteration process when the predefined objectives are reached with minimum errors with respect to the dose-volume histograms (DVHs) produced during iteration

The DVO optimization is generally influenced by the tissue heterogeneity existence and subjected to optimization convergence error [22-25]. In the DVO optimization, dose calculation errors are particularly present in the electronic disequilibrium region near the heterogeneity interfaces as is the case in our study. Finally, it is important to mention that medical physicists with the assistance of the clinician have to assign correct and optimal priority values to the optimization objectives of the PTV structures and OARs. The iteration is performed in a compromised way by tending the objectives on the OARs towards low doses and ensuring no significant impact on the DVH of the PTV at the same time. The priorities to be considered in this iteration process between PTV and OARs depend on the PTV dose coverage and homogeneity criteria previously defined by the clinician depending on the treated case [26].

Comparison between IMRT and 3D-CRT calculated and TL measured doses

In the present study, point-doses were measured by *ThermoFisher TLD-700* using the Risø TL/OSL-DA-20 reader [5,6]. Thermoluminescence signals were all collected under the same experimental conditions presented in Table 4. Therefore, the same 19 dose-measurement positions used for 3D-CRT were used for IMRT within the Rando phantom (Figure 1). The beams listed in Table 2 were delivered to Rando phantom according to the IMRT treatment plan. In this study, dose delivery comparison was performed in terms of experimental TL measured doses, as well as horizontal and vertical dose-profiles across heterogeneity media (spinal cord and right lung) showed in Figure 2 and DVHs.

Results

Point-dose measurement and comparison of the IMRT with 3D-CRT

The obtained TL-dose response curve is presented in Figure 3. This calibrated TL=f(D) curve allows the determination of absorbed dose within the interval between 0.1 and 2.5 Gy. All TLDs in the used batch were annealed together in an oven with the same

procedure and conditions as presented in Table 4. The reproducibility in dose measurement was found to be within an interval of $\pm 3\%$. The TL measured point-doses at different depths were compared to TPS calculated ones for 3D-CRT and IMRT (Table 5). Additionally, the difference between the calculated and the measured doses for both radiotherapy techniques was also evaluated. The TL-measured doses demonstrate normal high differences (Δ) versus calculated doses in case of low doses. All the differences between measured and calculated low doses ($<0.55\text{Gy}$) have mean values around 7% and 6.5% for IMRT and 3D-CRT, respectively.

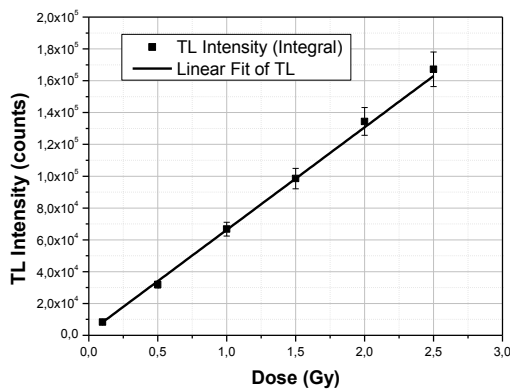


Figure 3. Response and calibration curve of used TLD dosimeters

On the other hand, the difference for higher doses ($>0.55\text{Gy}$) has a mean value of about 3 % for IMRT and

$\sim 1.0\%$ for 3D-CRT. The measured dose on the heart (position 2) was only 2 Gy in IMRT, whereas it was 5.4 Gy in 3D-CRT. The IMRT heart dose measured value is very comfortable regarding the constraints on OARs irradiation considered in the actual IMRT treatment planning. The measured doses on PTV for both radiotherapy techniques are globally in good agreement with the ICRU recommendations; however, the IMRT has a noticeable advantage over the 3D-CRT. In IMRT, all calculated and measured doses in the PTV (Table 6) were found to be within the interval of 95%-107% (1.9-2.14Gy) of the prescribed dose (2 Gy). Therefore, the PTV is well covered from a dose deposition point of view according to the validated IMRT treatment plans. The same statement is not valid for 3D-CRT since some very high deviations were observed on some dose measurement points (positions 11 and 15).

IMRT-DVO and heterogeneity correction

The tissue heterogeneity is an important aspect that needs to be considered in the dose optimization of radiotherapy treatment planning. Therefore, IRMT and 3D-CRT were compared regarding the calculated dose distributions across heterogeneous media. Accordingly, dose profiles were plotted across the mentioned horizontal scanning line passing through lungs (from right to left) and vertical scanning line passing through the spinal cord (from posterior to anterior sides) (Figures 4 and 5).

Table 5. Different anisotropic analytical algorithm-calculated doses for 3D-CRT and IMRT and thermoluminescence-measured doses and differences Δ between calculated and measured for 3D-CRT and IMRT (See Figure 1 for the location of TLDs)

TLD location	3D-CRT		IMRT		Dose Comparison	
	Calculated Dose (Gy)	Measured Dose (Gy)	Calculated Dose (Gy)	Measured Dose (Gy)	Δ (%)	Δ (%)
1	0.087	0.094 \pm 0.004	0.043	0.046 \pm 0.002	7.45	6.52
2	0.25	0.27 \pm 0.01	0.11	0.10 \pm 0.01	7.41	10
3	0.21	0.23 \pm 0.01	0.11	0.12 \pm 0.01	8.69	8.33
4	2.11	2.08 \pm 0.10	1.97	2.05 \pm 0.10	1.44	3.90
5	0.17	0.18 \pm 0.015	0.049	0.053 \pm 0.002	5.55	7.54
6	0.28	0.32 \pm 0.02	0.19	0.20 \pm 0.02	12.5	5
7	1.05	1.04 \pm 0.05	0.52	0.55 \pm 0.03	0.96	5.45
8	1.71	1.70 \pm 0.08	1.08	1.00 \pm 0.05	0.59	8
9	0.54	0.52 \pm 0.06	0.28	0.26 \pm 0.02	3.85	7.7
10	0.27	0.29 \pm 0.01	0.17	0.19 \pm 0.02	6.90	10.52
11	2.13	2.17 \pm 0.10	2.00	2.05 \pm 0.10	1.84	2.44
12	0.21	0.24 \pm 0.01	0.23	0.24 \pm 0.01	12.5	4.16
13	0.51	0.51 \pm 0.02	0.38	0.40 \pm 0.02	0	5
14	2.09	2.08 \pm 0.10	2.09	2.05 \pm 0.10	0.48	1.95
15	2.10	2.23 \pm 0.10	1.98	2.08 \pm 0.10	5.83	4.80
16	2.03	2.04 \pm 0.10	1.98	2.05 \pm 0.10	0.49	3.41
17	2.01	2.00 \pm 0.10	2.05	1.98 \pm 0.10	0.5	3.53
18	2.07	2.09 \pm 0.10	2.07	2.05 \pm 0.10	0.96	0.97
19	2.09	2.13 \pm 0.10	2.07	2.10 \pm 0.10	1.88	1.43

Table 6. Percentage (%) of the calculated doses and TL-measured doses concerning the prescribed dose (2Gy) for 3D conformal planning (3DCR) and IMRT optimized planning (IMRT).

PTV: planning treatment volume; HU: Hounsfield unit; TLD: thermoluminescence dosimeter; GTV: Gross tumor volume, see Figure 1 for the location of TLDs

TLD location	HU _{av} (Location)	% of the calculated / TL doses to prescribed dose 3D-CRT	% of the calculated / TL doses to prescribed dose IMRT
1	17.75(Heart)	4.4/4.7	2.15/2.4
2	19.75(Heart)	12.5/13.5	5.5/5.0
3	13.25(Heart)	10.5/11.5	5.5/6.0
4	25.75(Soft tissue, GTV)	105.5/104.0	98.5/102.5
5	-669(Left Lung)	8.5/9.0	2.5/2.75
6	10.5/-650* (Interface)	14.0/16.0	9.5/10.0
7	12.75(Soft tissue)	52.5/52.0	26.0/28
8	13.75(Soft tissue)	85.5/85.0	54.0/50.0
9	12.5(Soft tissue)	27.0/26.0	14.0/12.5
10	-476.25(Left Lung)	13.5/14.5	8.5/9.5
11	12(Soft tissue, GTV)	106.5/108.5	100/102.5
12	20/-433.5*(Interface)	10.5/12.0	11.5/12.5
13	22.5(Soft Tissue)	25.5/25.5	19.0/20.0
14	-469(PTV)	104.5/104.0	104.5/102.5
15	8/-705.75*(Interface)	105.5/111.5	99.0/104.0
16	-439.25(PTV)	101.5/102.0	99.0/102.5
17	-404(PTV)	100.5/100.0	102.5/99.0
18	-434.25(PTV)	103.5/104.5	103.5/102.5
19	-339.5(PTV)	104.5/106.5	103.5/105

*HUs of soft tissue/lung interface.

Table 7. Dose covering evaluation

Index	3D-CRT	IMRT
Conformity index	0.95	0.99
Heterogeneity index	0.112	0.085
Uniformity index	1.099	1.07

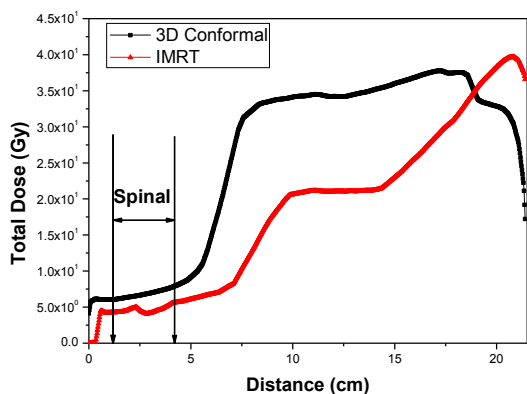


Figure 4. Vertical dose profile line showing calculated dose variation through the heterogeneous spinal cord medium

Concerning the spinal cord heterogeneity, the obtained results demonstrate the less exposure of this organ by IMRT by a maximum value of 32.5% on the considered dose profile line, compared to 3D-CRT. The dose profile just after the interface toward anterior direction increases considerably in 3D-CRT, compared to IMRT (Figure 4). For the left lung, the obtained results show that IMRT with its dose-volume optimization algorithm makes the dose profile less spread on the interfaces with

a more consistent fall in terms of dose before and after the heterogeneity interface (Figure 5).

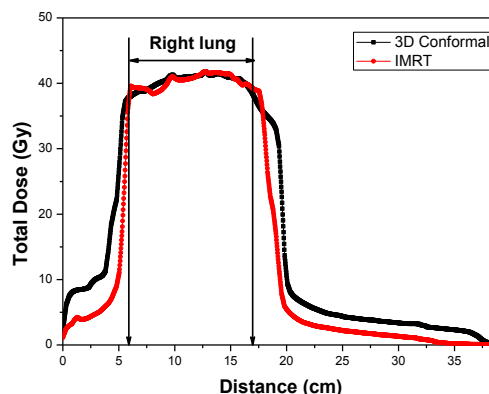


Figure 5. Horizontal dose profile line showing calculated dose variation through the heterogeneous right lung medium

In this study, the shape differences of the DVHs were also evaluated for IMRT and 3D-CRT (Figures 6 and 7). Although the main constraints on dose delivery are globally respected in both radiotherapy techniques, the deep analysis of the DVHs demonstrates that IMRT ensures a better PTV dose covering and an improved

OARs (left lung, spinal cord, and heart) exposure sparing. Therefore, it was demonstrated that the presence of large heterogeneities was entirely accounted for IMRT by the dose-volume optimizer, compared to 3D-CRT by the AAA with its heterogeneity correction method.

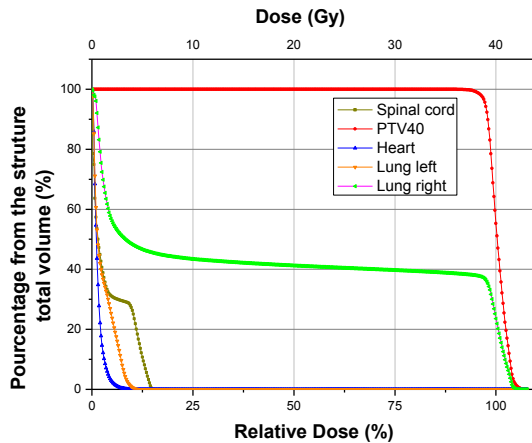


Figure 6. Dose-volume histograms calculated for the most important organs and volumes for the considered IMRT treatment planning

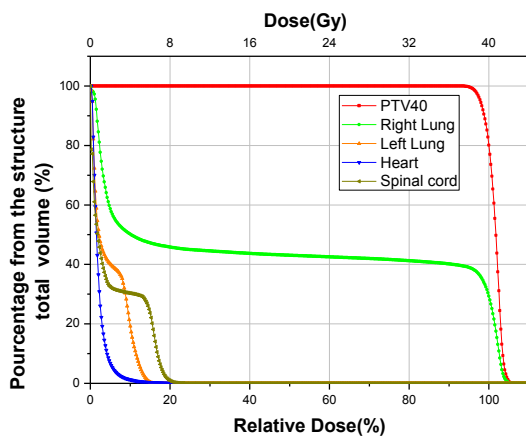


Figure 7. Dose-volume histograms calculated for the most important organs and volumes for the 3D conformal treatment planning

Moreover, effective exposure dose percentage reduction of 25.3%, 28.3%, and 41.55% was found for the spinal cord, heart, and left lung, respectively. In terms of the PTV dose covering, the comparison shows an insignificant difference (0.92%) between IMRT and 3D-CRT which proves that the PTV is well covered in terms of delivered dose concerning the prescribed dose in both techniques. The calculated dose converging indices presented in Table 7 confirm these findings.

Discussion

The treatment plan is significantly improved by IMRT according to this experimental point-dose measurement. In terms of local dose optimization, the TL measured point-dose shows a clear IRMT dose optimization, compared to 3D-CRT. Experimental results demonstrate that the local dose at the level of the

heart is reduced by more than 50%. The dose near the spinal cord is also decreased by about 20% in IMRT.

However, the measured dose delivered to the PTV is more accurate and is found within an interval of $\pm 5\%$ of the prescribed dose for all the measurement positions. It is important to mention that our TL dose measurement in all considered points showed dose overestimation and underestimation by both IMRT and 3D-CRT with most differences within a tolerable interval. It is worth mentioning that high deviations were observed for points 11 (+6.5 %) and 15 (+5.5%) in 3D-CRT.

All the calculated indices are favorable for a better IMRT dose covering, compared to the 3D-CRT. Close collaboration between clinician and medical physicist is more than necessary to reach the predefined objectives of dose delivery with IMRT. The IMRT relies on computerized inverse planning; therefore, OARs need to be accurately contoured to instruct the system to avoid depositing high dose in these tissues. Since the IMRT implementation to date, 126 patients were treated for head and neck and 21 ones for brain cancers at the CLCC radiotherapy service. The CLCC radiotherapy service is advised to start the implementation of breathing motion reduction and respiratory gating techniques in order to extend the use of IMRT to lung cancer, particularly in case of complex clinical situations. This is because the actual study on Randon phantom demonstrates well the ability of IMRT to ensure an efficient treatment in terms of dose conformity and OARs effective sparing, compared to 3D-CRT for such cases.

Finally, it should be mentioned that in addition to our study, IMRT with its dose optimization was studied for the treatment of lung and other very specific cancers. According to a study conducted by Michael J. Chen et al., the treatment of lung cancer with IMRT instead of 3D-CRT improved the physical and biological conformability of the dose delivery [27]. They also noticed a possible higher dose delivery to the hypoxic target volume avoiding the use of a higher number of fractions leading to the less exposure of the healthy tissues. Chen et al. also confirmed that IMRT was more appropriate than 3D-CRT for the treatment of lung cancer with large tumor volumes and locations not easily accessible to radiotherapy [27].

Concerning radiotoxicity, it is also mentioned in this study that based on recent retrospective studies, more than a triple number of esophagitis patients treated with 3D-CRT require a feeding tube than those treated with IMRT ($P=0.005$). In the same context, another retrospective study on the evaluation of 5-year survival rates shows a value of 14% for IMRT or 3D-CRT compared to a value of 11% for conventional radiotherapy ($P=0.0001$) [27].

It was also observed by Chan et al. [28] that according to many studies [29-35], IMRT was able to reduce the volume of lung receiving more than 20 Gy (V_{20}). These studies observe that the effect of IMRT on lower dose-volumes in lung DVH is not well elucidated. Some studies observe a reduction of V_5 [30,34],

whereas other studies state an increase in this regard [32,33,36]. Chen et al. revealed that the majority of the studies demonstrated the IMRT advantage for the heart and spinal cord exposure [32, 33, 35-38]. In the same line, Boyle et al. demonstrated that the IMRT was able to decrease dose to be delivered to the lungs, heart, and esophagus with an equivalent coverage of the PTV and better therapy tolerability, compared to 3D-CRT [39]. Another more recently conducted study showed that IMRT ensured better 5-year overall survival than 3D-CRT with a significant predictive factor, particularly for advanced primary tumors [40]. Regarding different cases other than lung cancer, C. Fiandra et al. [41] indicated that IMRT was a very effective radiotherapy technique with its capability of target volume coverage, as well as OARs and healthy tissues sparing in early-stage Hodgkin's lymphoma.

Conclusion

This study revealed that IMRT guaranteed better protection of the OARs and accurate treatment planning through its dose optimization DVO algorithm, compared to 3D-CRT. It has been well demonstrated that IMRT with its DVO has well enhanced the dose coverage of the PTV. Moreover, the complex case of lung cancer with a PTV surrounded by heterogeneities constituted a difficult case of treatment and a serious test to the IMRT after its implementation. Therefore, the IMRT can be applied to improve the treatment toxicity in lung cancer and avoid side effects by better protection and low dosage of the healthy lung, esophagus, heart, and spinal cord. For the considered lung cancer treatment with 6 MV 3D-CRT and field sizes greater than $10 \times 10 \text{ cm}^2$, it was observed that AAA tended to underestimate the dose in the lung and overestimate it in the tissue located just after the lung. Regarding IMRT, the findings of this study demonstrated that IMRT can deliver prescribed dose safely with acceptable accuracy and less toxicity. At the CLCC radiotherapy service, IMRT is now used for patients unable to meet 3D-CRT dose constraints and those who would have been expected to have lower survival. Based on the results of this study, as well as our recommendations, the treatment extension to lung cancer treatment will be completely ensured shortly after the implementation of breathing motion reduction and respiratory gating techniques.

Acknowledgment

This study was supported by the General Direction of Scientific Research and Technological Development (DGRSDT) of the Algerian Higher Education and Scientific Research Ministry. The principal investigator and his research team would like to thank DGRSDT for its support in the achievement of this project.

References

1. Bouacid SS, Kharfi F, Boulakhssaim F. Comparison of measured and calculated doses in a Rando phantom with a realistic lung radiotherapy treatment

- plan including heterogeneities. *Radiat Environ Biophys.* 2018 Sep 11; 57:365-73.
2. Landberg T, Chavaudra J, Dobbs J, Gerard JP, Hanks G, Horiot JG, et al. Report 62: Prescribing, Recording and Reporting Photon Beam Therapy (Supplement to ICRU report 50). *Journal of the ICRU.* 1999 Nov 1; 32 (1).
3. Landberg T, Chavaudra J, Dobbs J, Hanks G, Johansson KA. Report 50: Prescribing, Recording and Reporting Photon Beam Therapy. *Journal of the ICRU.* 1993 Sept 1; 26 (1).
4. Varian medical system: Eclipse Algorithms Reference Guide. P/N B502612R03A, Palo Alto. 2009.
5. Kharfi F, Ketfi R. Irradiated black pepper identification based on thermoluminescence of silicate minerals. *J Radioanal Nucl Chem.* 2018 Jan 11; 315:503-7.
6. DTU Nutech. Denmark. Guide to the Risø TL/OSL Reader. 2015. Available from: <https://www.usu.edu/geo/luminlab/Reader.pdf>.
7. Vol I. Prescribing, Recording, and Reporting Photon-Beam Intensity-Modulated Radiation Therapy (IMRT): Contents. *Journal of the ICRU.* 2010 Apr; 10(1).
8. Feuvret L, Noel G, Mazeron JJ, Bey P. Conformity index: a review. *Int J Radiat Oncol Biol Phys.* 2006 Feb 1; 64(2):333-42.
9. Sheng K, Molloy JA, Larner JM, Read PW. A dosimetric comparison of non-coplanar IMRT versus Helical Tomotherapy for nasal cavity and paranasal sinus cancer. *Radiother Oncol.* 2007 Feb; 82(2):174-8.
10. Oelfke U, Nill S, Wilkens JJ. Physical optimization. *InImage-guided IMRT.* 2006.
11. Lu R, Radke RJ, Yang J, Happersett L, Yorke E, Jackson A. Reduced-order constrained optimization in IMRT planning. *Physics in Medicine & Biology.* 2008 Nov 7;53(23):6749.
12. Xing L, Li J, Donaldson S, Le Q, Boyer A. Optimization of importance factors in inverse planning. *Phys Med Biol.* 1999 Oct; 44(10):2525-36.
13. Lu R, Radke R, Happersett L, Yang J, Chui C, Yorke E, et al. Reduced-order parameter optimization for simplifying prostate IMRT planning. *Phys. Med. Biol.* 2007 Jan 17; 52:849-70.
14. Webb S. Optimisation of conformal radiotherapy dose distributions by simulated annealing. *Phys Med Biol.* 1989 Oct; 34(10):1349-70.
15. Morrill S. M., Lane R. G., Jacobson G, Rosen II. Treatment planning optimization using constrained simulated annealing. *Phys Med Biol.* 1991 Oct; 36(10):1341-61.
16. Webb S. Optimization by simulated annealing of three-dimensional, conformal treatment planning for radiation fields defined by a multileaf collimator: II. Inclusion of two-dimensional modulation of the x-ray intensity. *Phys Med Biol.* 1992 Sep; 37 (8):1689-704.
17. Bortfeld T. Optimized planning using physical objectives and constraints. *Semin Radiat Oncol.* 1999 Jan; 9(1):20-34.
18. IMRTCWG. Intensity-modulated radiotherapy: current status and issues of interest. *Int J Radiat Oncol Biol Phys.* 2001 Nov 15; 51(4):880-914.
19. Vanetti E, Nicolini G, Nord J. On the role of the optimization algorithm of Rapid Arc volumetric

- modulated arc therapy on plan quality and efficiency. *Med Phys.* 2011 Nov; 38(11):5844-56.
20. Zacarias AS, Mills MD. Algorithm for correcting optimization convergence errors in Eclipse. *J Appl Clin Med Phys.* 2009 Oct 14; 10(4):3061.
 21. Holmes T, and Mackie TR. A comparison of three inverse treatment planning algorithms. *Phys Med Biol.* 1994 Jan; 39(1):91-106.
 22. Jeraj R, Keall PJ, Sieber JV. The effect of dose calculation accuracy on inverse treatment planning. *Phys Med Biol.* 2002 Feb 7;47(3):391-407.
 23. Jeraj R, Wu C, Mackie TR. Optimizer convergence and local minima errors and their clinical importance, *Phys Med Biol.* 2003 Aug 12; 48(17):2809-27.
 24. Dogan N, Siebers JV, Keall PJ, Lerma F, Wu Y, Fatyga M, et al. Improving IMRT dose accuracy via deliverable Monte Carlo optimization for the treatment of head and neck cancer patients. *Med Phys.* 2006 Nov; 33(11):4033-43
 25. Mihaylov IB, Siebers JV. Evaluation of dose prediction errors and optimization convergence errors of deliverable-based head-and-neck IMRT plans computed with a superposition/convolution dose algorithm. *Med Phys.* 2008 Aug; 35(8): 3722-7.
 26. Tol JP, Dahele M, Doornaert P, Slotman BJ, Verbakel WF. Different treatment planning protocols can lead to large differences in organ at risk sparing. *Radiother Oncol.* 2014 Nov; 113(2):267-71.
 27. Chen MJ, Novaes PE, Gadia R, Motta R. Guidelines for the treatment of lung cancer using radiotherapy. *Rev Assoc Med Bras.* 2017 Sep; 63(9):729-32.
 28. Chan C, Lang S, Rowbottom C, Guckenberger, M, Faivre-Finn C. Intensity-modulated radiotherapy for lung cancer: current status and future developments. *J Thorac Oncol.* 2014 Nov; 9(11):1598-608.
 29. Murshed H, Liu HH, Liao Z, Barker JL, Wang X, Tucker SL, et al. Dose and volume reduction for normal lung using intensity-modulated radiotherapy for advanced-stage non-small-cell lung cancer. *Int J Radiat Oncol Biol Phys.* 2004 Mar 15;58(4):1258-67.
 30. Zhang GG, Ku L, Dilling TJ, Stevens CW, Zhang RR, Li W, et al. Volumetric modulated arc planning for lung stereotactic body radiotherapy using conventional and unflattened photon beams: a dosimetric comparison with 3D technique. *Radiat Oncol.* 2011 Nov 9 ;6:152.
 31. Cattaneo GM, Dell'oca I, Broggi S, Fiorino C, Perna L, Pasetti M, et al. Treatment planning comparison between conformal radiotherapy and helical tomotherapy in the case of locally advanced-stage NSCLC. *Radiother Oncol.* 2008 Sep; 88(3):310-8.
 32. Chan OS, Lee MC, Hung AW, Chang AT, Yeung RM, Lee AW. The superiority of hybrid-volumetric arc therapy (VMAT) technique over double arcs VMAT and 3D-conformal technique in the treatment of locally advanced non-small cell lung cancer-a planning study. *Radiother Oncol.* 2011 Nov;101(2):298-302.
 33. Liu HH, Wang X, Dong L, Wu Q, Liao Z, Stevens CW, et al. Feasibility of sparing lung and other thoracic structures with intensity-modulated radiotherapy for non-small-cell lung cancer. *Int J Radiat Oncol Biol Phys.* 2004 Mar 15; 58(4):1268-79.
 34. McGrath SD, Matuszak MM, Yan D, Kestin LL, Martinez AA, Grills IS. Volumetric modulated arc therapy for delivery of hypofractionated stereotactic lung radiotherapy: A dosimetric and treatment efficiency analysis. *Radiother Oncol.* 2010 May; 95(2):153-7.
 35. Christian JA, Bedford JL, Webb S, Brada M. Comparison of inverse planned three-dimensional conformal radiotherapy and intensity-modulated radiotherapy for non-small-cell lung cancer. *Int J Radiat Oncol Biol Phys.* 2007 Mar 1;67(3):735-41.
 36. Bree Id, van Hinsberg MG, van Veelen LR. High-dose radiotherapy in inoperable nonsmall cell lung cancer: comparison of volumetric modulated arc therapy, dynamic IMRT and 3D conformal radiotherapy, *Med Dosim.* 2012 Mar 28; 37(4):353-7.
 37. Ong CL, Verbakel WF, Cuijpers JP, Slotman BJ, Lagerwaard FJ, Senan S. Stereotactic radiotherapy for peripheral lung tumors: a comparison of volumetric modulated arc therapy with 3 other delivery techniques. *Radiother Oncol.* 2010 Dec; 97(3):437-42.
 38. Simeonova A, Abo-Madyan Y, El-Haddad M, Welzel G, Polednik M, Boggula R, et al. Comparison of anisotropic aperture based intensity modulated radiotherapy with 3D-conformal radiotherapy for the treatment of large lung tumors. *Radiother Oncol.* 2012 Feb; 102(2):268-73.
 39. Boyle J, Ackerson B, Gu L, Chris R, Kelsey R. Dosimetric advantages of intensity modulated radiation therapy in locally advanced lung cancer. *Adv Radiat Oncol.* 2017 Jan-Mar; 2(1): 6-11.
 40. Moon SH, Cho KH, Lee CG, Keum KC, Kim YS, Wu HG, et al. IMRT vs. 2D-radiotherapy or 3D-conformal radiotherapy of nasopharyngeal carcinoma. *Strahlenther Onkol.* 2016 Jun; 192(6):377-85.
 41. Fiandra C, Filippi AR, Catuzzo P, Botticella A, Ciammella P, Franco P, et al. Different IMRT solutions vs. 3D-Conformal Radiotherapy in early stage Hodgkin's lymphoma: dosimetric comparison and clinical considerations. *Radiat Oncol.* 2012 Nov 2; 7:186-95.